Accuracy of CFD Simulations on Indoor Air Ventilation: Application of Grid Convergence Index on Underfloor Air Distribution (UFAD) System Design

Nor Azira Mohd Zainuddin, Fauziah Jerai[*]*, Azli Abd Razak, Mohd Faizal Mohamad*
School of Mechanical Engineering, College of Engineering, Universiti Teknologi MARA, 40450, Shah Alam, Selangor, MALAYSIA
[*]*fauziahjerai@uitm.edu.my*

ABSTRACT

Underfloor air distribution system (UFAD) mesh flow velocity was simulated using Computational Fluid Dynamics (CFD). Three mesh sizes were used to explore the domain's core x-y plane velocity contour and profiles. Compared to medium and fine, the coarse mesh underestimated the velocity significantly. A slight discrepancy occurred where the shear flow was dominant. The symmetrical flow velocity for both sides of the room length was shown in the xy-plane at the centre of the inlet. The mean error for coarse and medium mesh was larger than for the medium and fine mesh. It shows that the difference between the medium mesh and the fine was accepted. The computational time for medium mesh was acceptable for simulation, and it will not vary substantially even if the grid is refined further. The normalised mean square error (NMSE), the factor of two observations (FAC2), the factor of 1.3 observations (FAC1.3), and the fractional bias (FB) are used to measure the performance of the models and the value of the outcomes was exceptional. As a result, the accuracy of the finding can be improved by conducting additional research with manikins and in a fully occupied room under real-world conditions. In addition, this study could analyse and anticipate the optimal scenario regarding ventilation performance, etc.

Keywords: *Computational Fluid Dynamics (CFD); Discretization Error; Grid Convergence Index (GCI); Mesh Refinements; Verification*

ISSN 1823-5514, eISSN 2550-164X

https://doi.org/10.24191/jmeche.v20i3.23908

Received for review: 2022-12-12
Accepted for publication: 2023-06-05
Published: 2023-09-15

Introduction

An underfloor air distribution (UFAD) system is used in many modern commercial buildings, like open office buildings because it is considered an energy-efficient way to move air. To prevent cold draughts and UFAD short-circuits, it is important to control the supply air's temperature and velocity. This could reduce the efficiency of new commercial buildings to remove heat generated by a highly sensible cooling load [1]-[2]. The UFAD indoor air distribution system may improve thermal comfort, air quality, and HVAC energy usage [3].

Displacement ventilation (DV) operates like UFAD systems for cooling. In cooling mode, DV and UFAD systems draw cold air from the floor and exhaust it from the ceiling. Thermal plumes from overheated sources cause floor-to-ceiling air movement by entraining and lifting air. High heat loads are accommodated through buoyancy-driven airflow. Its thermal plume cools the room. DV and UFAD deliver space air differently. UFAD diffusers mix more than DV diffusers, which are low-velocity. This lets a reduced air volume supply meet room load. Air rising in the room uses heat gain's natural buoyancy in space to generate a vertical temperature differential. Due to differing fluid dynamics, UFAD can have a lower supply air temperature and higher flow rate than DV [4].

Indoor environments are frequently modelled using Computational Fluid Dynamics (CFD) [5]-[7]. CFD simulations require accurate computational mesh and flow problem physics. In CFD models, input models and numerical uncertainty might influence the numerical solutions. The accuracy is linked with the grid resolution. For example, spatial discretization error is the most challenging and demanding approximation. The discretization error can be decreased by refining the grid. Increasing discretization scheme order and mesh size or quality reduces numerical errors. When raising mesh resolution, it is necessary to consider all elements affecting mesh quality. Uniformity, aspect ratio, orthogonality, and skewness values are essential mesh qualities to examine. These mesh metrics will affect the solution method's accuracy, robustness, and efficiency; therefore, whether a mesh is good or bad depends on the numerical discretization. Getting a solution that does not rely on the mesh size can be very expensive and take a long time, significantly if the mesh size is reduced randomly. Finding the proper mesh density for a given problem has proven challenging while maintaining computational time and accuracy within acceptable limits. Making a well-distributed mesh from the start can save from using adaptive mesh techniques, and it is essential to set the correct values at the beginning.

Other than that, CFD modelling is difficult for ventilation when developing unstable turbulence models like Large Eddy Simulation (LES) and representing inlet boundary conditions. The challenge is predicting internal airflow and ventilation. Reynolds-averaged Navier–Stokes (RANS) or

Unsteady RANS (URANS) equations are extensively employed for ventilation simulation due to their inexpensive cost, but their accuracy is restricted by unresolved temporal turbulent fluctuations, an assumption of Reynolds stress isotropy, and low-Reynolds-number effects. RANS models were not designed to forecast flow regimes like boundary layer separation [8]. RANS models overestimate turbulent dissipation, which raises wall shear stress, delays the separation of the wall boundary layer, and misaligns the wall jet. These issues may make it difficult to anticipate air flow and turbulence, which is crucial for removing indoor pollutants. Building ventilation systems aren't optimised by RANS models. Owing to RANS's constraints, we need to improve the numerical equations and apply the right LES models for ventilation simulations while considering low-Reynolds-number effects [9].

Most indoor CFD models use hexahedral, tetrahedral, or hybrid meshes [10]-[11]. The hexahedral mesh can be structured or unstructured, but the other two are not structured. Several CFD studies have looked at how mesh types and cell shapes affect the mean flow profile. The grid independence test was utilised in various ways while examining the indoor environment. There is a structured and unstructured mesh. The structured mesh comprises two main types: regular topology and repeated primitive shapes in space. For structured meshes, flow-aligned hexahedral elements can improve solution accuracy with a small number of cells but making the mesh topology may take time. For unstructured, the connections between the vertices are not regular, and there is no any underlying shape repetition. These meshes are more flexible, easier to make and saves time. However, it may need more cells to be as accurate as structured meshes [12].

Researchers have modelled particle movement and settlement in indoor environments using Mixing Ventilation (MV), Displacement Ventilation (DV), and Underfloor Air Distribution (UFAD) systems. Semi-empirical deposition models explain how particles build up at solid boundaries. The size-dependent deposition characteristics are well figured out in these models, which are used to facilitate the rules [5]. A semi-empirical expression in the range of particle sizes from 0.01-10 µm is compared to an existing numerical model. The deposition and fate of particles are depicted, and a positive outcome is only possible if the near-wall grid is sufficiently small and the turbulent kinetic energy near the wall is adequately muted depending on its component normal to the wall [6].

Before creating our mesh, we must establish the optimal mesh type for our case. In addition, it substantially impacts the cost and accuracy of CFD simulations. Numerous CFD studies have done grid independence evaluations to assess their performance. A spatial discretization error may occur if the mesh is too large or small. Through mesh refinement, the numerical dissipation may be minimized. In addition, a large grid number could be damaging. If the round-off error is huge, it might quickly exceed the truncation error, resulting in decreased accuracy. There may be adverse outcomes if the number of cells

in a cell is too few or too many. Therefore, it is essential to determine the optimal grid number [13].

This study aims to figure out the Grid Convergence Index (GCI) for indoor airflow of an underfloor air distribution (UFAD) system with three different grid resolutions. It is the most common and accurate way to figure out how uncertain the result is. The goal is to determine how the mesh resolution affects the order of accuracy and numerical solution accuracy. It is based on the lower accuracy limit, which can lead to incorrect conclusions when the observed accuracy order differs from the formal order of accuracy [14]. Three kinds of uncertainty can affect the numerical solutions: uncertainty in the inputs, the model, and uncertainty in the math itself. These include spatial and temporal discretization, convergence, and rounding errors [15]. There are many different approximations, but one of the most important and hardest is the error that comes with a grid resolution or spatial discretization error. Grid refinement can be used to reduce the error that comes from discretization. Adjusting the mesh and discretization step size helps reduce numerical errors. All elements that degrade mesh quality when resolution is increased must be considered.

A study compared simulated airflow and temperature distributions in a first-class cabin with the variables (hexahedral, tetrahedral, and hybrid cells) was done in 2015. The study discovered that hexahedral meshes were the most precise, but also the most expensive to compute [16]. In addition, it looked at how mesh refinement and cell topology changed the indoor airflow profile by looking at a graph between the data and the results from computer simulations but not quantitatively.

Grid Convergence Index (GCI) was used [17]-[20] to look at how mesh resolution and cell geometry predict outdoor environments, like how pollutant gas spreads around buildings. The grid resolution affects the accuracy of numerical results by looking at how indoor air temperature changes over time and how old the air is [21]-[22]. Instead, some researchers looked at temperature and velocity profiles. When calculating the velocity flow profile, the hexahedral mesh outperforms the tetrahedral mesh but also took the most time to make. The hybrid meshes were the least accurate but took the least amount of time to calculate. By increasing the number of grids in the hybrid mesh to get the same level of accuracy as with hexahedral meshes, the same amount of time is spent on computing. From the study, the accuracy of simulations with hexahedral meshes with 12 million cells, hybrid meshes with 24 million cells, and tetrahedral meshes with about 15 million cells would be the same. Also, each of these simulations would take about 80–90 hours to run on the computer network [16].

By adding more grids to the hybrid mesh, accuracy can be increased. Hexahedral mesh matches experimental data faster than other mesh designs [21], [23]-[24]. The GCI method can figure out the order of convergence and the asymptotic answer in a solid way. Even though more study needs to be

done on blast situations and finite element (FE) calculations, this method seems to be a good estimate. Researchers can analyse the airflow, air quality, and thermal comfort by using a good simulation to predict the real airflow, air quality, and thermal comfort data. This study identifies the optimal mesh size that could rank the error based on how far off the key predicted and measured results were from each other. A study of air velocity distributions showed that different mesh types led to different simulation results due to truncation problems.

Methodology

Model development

Most buildings are ventilated either mechanically, naturally, or both. Airflow within rooms is often turbulent, and turbulence disperses particles more efficiently. Before figuring out how particles move, it is important to know how the air flows around them. The Eulerian method is used to simulate the air in this numerical analysis. A new drift–flux model is used to solve the turbulent airflow field utilising the Renormalization Group (RNG) k-turbulence model as validated by paper [10]. RNG *k-ε* models simulate three-dimensional (3D) turbulent airflow [25]. They are computationally efficient and stable compared to seven-equation Reynolds stress models. RNG and traditional *k–ε* models have different constant coefficients despite similar formulations. Compared to the standard *k–ε* model and other turbulence or laminar models [26], the RNG *k–ε* model is more suited for simulations of indoor airflow. The general version of the governing Equation (1) for an incompressible fluid is as follows:

$$\frac{\partial y}{\partial x}(\varphi) + \nabla.(u_{\varphi}) = \nabla.(\tau_{\varphi}\nabla_{\varphi}) + S_{\varphi} \quad (1)$$

u is the velocity vector, ϕ represents each of the three velocity components, *u*, *v*, and *w*. τ_{φ} is the effective diffusion coefficient φ. S_{φ} is the source term of the general Equation (2). When S_{φ}=1, the Equation changes into the continuity equation.

Most airflows indoors are turbulent. So, turbulence modelling is essential for most CFD simulations [27]. Reynolds-Averaged Navier-Stokes (RANS) turbulence modelling has become a popular way to model how air moves in closed spaces. For indoors, the air phase flow is viscous, incompressible, isothermal, and has the same density. RNG k ε turbulence model has been used with the Reynolds-Averaged Navier-Stokes (RANS) equations as a guide. They can be written down in general terms:

$$\rho\bar{u}j\,\frac{\partial\bar{u}_i}{\partial x_j} = \rho\bar{f}_i + \frac{\partial}{\partial x_j}\left[-\rho\delta_{ij} + \mu\left(\frac{\partial\bar{u}_i}{\partial x_j} + \frac{\partial\bar{u}_j}{\partial x_i}\right) - \rho\overline{u'_i\,u'_j}\right] \quad (2)$$

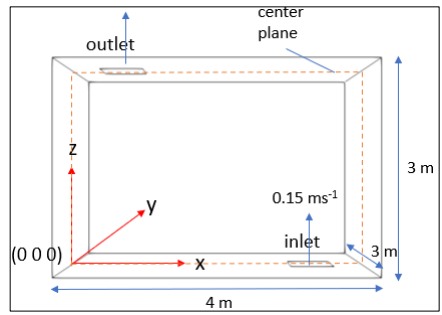

Figure 1: The sectional perspective of the room geometry used for the development of the indoor airflow profile model

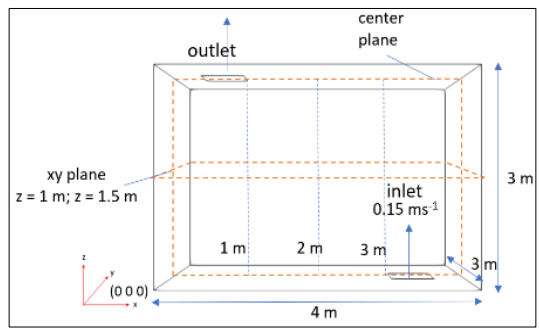

Figure 2: The centre plane of the model

Figure 1 shows the sectional perspective of the room geometry, where width (*W*) x height (*H*) x length (*L*) = 4 x 3 x 3 m. Figure 2 shows the centre of each *xy*-plane and the *xz*-plane for the domain. The inlet and outlet dimensions are 0.6 x 0.6 m (refer to JKR dwg. std) and are located on the floor and at the top.

Boundary condition

Boundary conditions specify the set of computational mesh faces that align with the physical domain's edges. There are two different kinds of boundary conditions: numerical and physical. Von Neumann and Dirichlet boundary conditions are the two forms of numerical boundary conditions. These boundary conditions affect the gradient along the border and the value on the

boundary (or a constant value) of the variable [28]. Below is the description of the physical boundary conditions for an incompressible flow:

i. Inlet: the velocity value is determined, and a zeroGradient pressure condition is set.
ii. Outlet: the outflow border is specified in the same manner as the total mass balance. The pressure distribution is specified, and the pressure and velocity boundary conditions are fixed to fixedValue and zeroGradient, respectively.
iii. Non-slip wall: the flow velocity on the wall is the same as the wall's velocity. As there is no flow through the wall, the pressure gradient is set to zeroGradient.

Three different patches in the computational domain have been made for this study. A part of the top surface is an outlet, while a part of the bottom surface is an inlet. The side surface is sometimes known as a wall. At the inlet patch, a fixedValue boundary condition is established, whereas, at the wall patch, a zeroGradient is applied. Tables 1 and 2 provide further information on boundary conditions. The industry Code of Practice on Indoor Air Quality (DOSH 2010) [29] has an acceptable range such as:

i. Air Temperature: 23 – 26 °C
ii. Relative Humidity: 40 – 70%
iii. Air Movement: 0.15 – 0.5 ms-1

The parameters input is referred to DOSH to make it as actual conditions to get the ideal values.

Table 1: Boundary conditions

Flow of Properties	Type of Patches		
	Outlet	Inlet	Walls
U	zeroGradient	fixedValue	fixedValue
K	zeroGradient	zeroGradient	kqRWallFunction
P	fixedValue	zeroGradient	zeroGradient
nuT	zeroGradient	zeroGradient	nutkWallfunction
ε	zeroGradient	fixedValue	epsilonWallFunction

Table 2: Explanation of boundary conditions

Type	Description of boundary conditions
zeroGradient	Normal gradient of ϕ is zero
fixedValue	Value of ϕ is specified
nutkWallfunction	On corresponding patches in the turbulent fields k and nut
kqRWallFunction	On corresponding patches in the turbulent fields k, q, and R
epsilonWallFunction	On corresponding patches in the epsilon field

Grid Convergence Index (GCI)

A discretization error is made in the simulation when a finite time and space domain is used. So, a number answer can only be thought of as a close estimate of the real answer. Grid Convergence Index (GCI) uses the mesh size to figure out how big this error is. The GCI first released Roache in 1994 [30]. This distance between our computed value and the asymptotic value can be thought of as the relative error bound. Users can see how big of an error that might be making and where it might fall inside the error band. While low GCI values indicate that the computational solution is close to the asymptotic on the mesh size, this also demonstrates how much the solution will vary when the mesh size is refined [30], [31]-[32]. If the solution is already good enough, making the mesh smaller will not make it much different. Some authors have shown that it is not always true the results are better when the mesh is finer [33]-[34]. Based on that idea, generally, the results are better when the mesh is finer. Compared to other methods, this one has some significant advantages since it does not need an analytical solution, gives a confidence limit for the estimated error band, and can be used with as few as two mesh solutions.

In the past, the exact analytical solution was used to find the convergence error, and then a graph was used to show the range of convergence. However, most real-world problems do not have clear answers. Most traditional discretization methods presume an exact solution f_{exact} and its numerical approximation *f(h)*. The discretization error is calculated using Equation (3), *E(h)*, and ignores higher-order terms when the mesh is fine enough [30], [35]-[36]:

$$E\,(h) = f_{exact} - f\,(h) \approx Ah^p \tag{3}$$

where h is a measure of the mesh's discretization, *A* is a constant, and *p* is the convergence rate. So, three unknowns are left: the constant *A*, the convergence ratio *p*, and the exact solution f_{exact}. The GCI method is based on figuring out these unknowns and estimating them. GCI was employed with three mesh refinements and a constant grid refinement ratio. The meshes used for this study (called A, B, and C) resulted in the following ratio, $r=h_A/h_B=h_B/h_C=2$.

Applying Equation (3) to mesh sizes A, B, and C estimates the order of convergence, where $h_A > h_B > h_C$. Then, the unknown constant *A* can be eliminated, and the unknown *p* can be obtained [37]:

$$p = \frac{\ln\left(\frac{f_A - f_B}{f_B - f_C}\right)}{\ln(r)} \tag{4}$$

The analytical conclusion can be approximated by utilising ABC's two best grids to get the asymptotic solution for *h* approaching zero since the order of convergence is known:

$$f_{h\to 0} \approx f_{exact} \approx f_A - \frac{f_B - f_C}{{r_{CB}}^p - 1} \tag{5}$$

Equation (5) calculates the relative error (ε) of finer meshes to mesh (r) and convergence (p) ratios [37]-[38]. The definition of the relative error is as follows:

$$\varepsilon_{CB} = \frac{f_B - f_C}{f_C} \tag{6}$$

which should never be used since the formula does not incorporate r or p. Equation (7) gives the GCI error as a percentage.

$$GCI_{CB} = F_S \frac{\varepsilon_{CB}}{{r_{CB}}^p - 1} \tag{7}$$

F_S calculates the safety factor by multiplying the relative error term from GCI scenarios. As the exact solution is unclear, this error estimates the finest mesh employed relative to the numerically converged solution [30]. This factor has a value of 3 when two meshes are analysed, and 1.25 when three or more meshes are analysed. The second value was utilised in this investigation. This safety factor indicates the degree of confidence that the calculated error bound is within 95%. Last but not least, the extrapolated (or computed) solution, denoted f^*_{CB} for the finer mesh combination, gives an approximation of the numerically asymptotic solution:

$${f^*}_{CB} = \frac{{r_{CB}}^p \cdot f_A - f_B}{{r_{CB}}^p - 1} \tag{8}$$

This approach is only applicable when all grids fall inside the asymptotic range, at which point Equation (8) is asymptotically true (also the solution that can be extrapolated to other mesh combinations). By comparing two GCI values from three meshes, the asymptotic range of convergence can be determined. This is based on the assumption that the ratio between errors and mesh spacing must be constant for the asymptotic range of convergence to be fulfilled [38].

$$GCI_{BA} \approx r^p GCI_{CB} \tag{9}$$

Lastly, since the GCI only gives the error bound, Equation (10) shows how to get the range that the converged solution should be within a 95% certainty.

$$|f_C(1-\frac{GCI_{CB}}{100\%}), f_C(1+\frac{GCI_{CB}}{100\%})| \quad (10)$$

Results and Discussion

Validation with Chen et al. [10] simulation

The accuracy of this work is judged by comparing steady-state simulation to scale-modeling data for a basic model room conducted by Chen et al. [10]. The characteristics of the CFD model, including the computational grid, turbulence model, boundary conditions, and near-wall treatment, are used to establish a trustworthy CFD model for validation research. The geometry and condition of their experimental setup are the same as our CFD setup. To validate the precision of airflow estimates, the x-direction velocity is compared to the experimental data reported by Chen et al. [10]. The model geometry done by Chen et al. is shown in Figure 3 in length (*x*), width (*y*), and height (*z*); 0.8 m, 0.4 m, and 0.4 m. Its inlet and outlet are the exact sizes, 0.04 x 0.04 m.

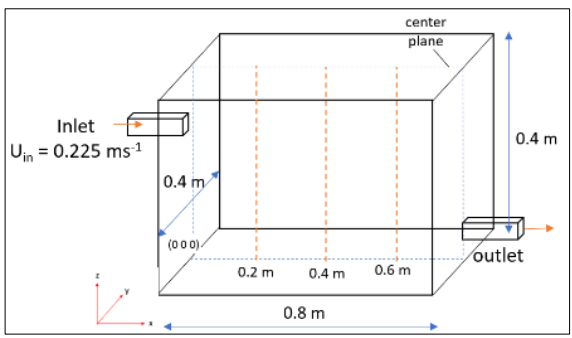

Figure 3: Ventilation chamber and experiment diagram by Chen et al. [10]

Two grid systems with 40 20 20 and 80 40 40 grids have been used with the grid-independent test. The comparison shows that the difference is not very big (less than 5%), and grid 40 20 20 is used. Velocity profiles at *x*=0.2 m, 0.4 m, and 0.6 m are compared with the experimental and simulation results. Inlet velocity is 0.225 ms^{-1} (corresponding to air change rates of 10 h-1). Chen's simulation is performed on an SGI Onyx 3800, and the solver used is the SIMPLER algorithm to couple the pressure and velocity fields [10]. The present simulation is done in OpenFOAM, and the solver is SIMPLE, which gives suitable velocity corrections; however, the pressure correction is less accurate [23], [39].

Figure 4 shows the graph of Chen's experiment, Chen's simulation, and the present simulation which compares the calculated velocity field with

experimental records in the x-direction at x=0.2 m, x=0.4 m, and x=0.6 m of the centre plane [10].

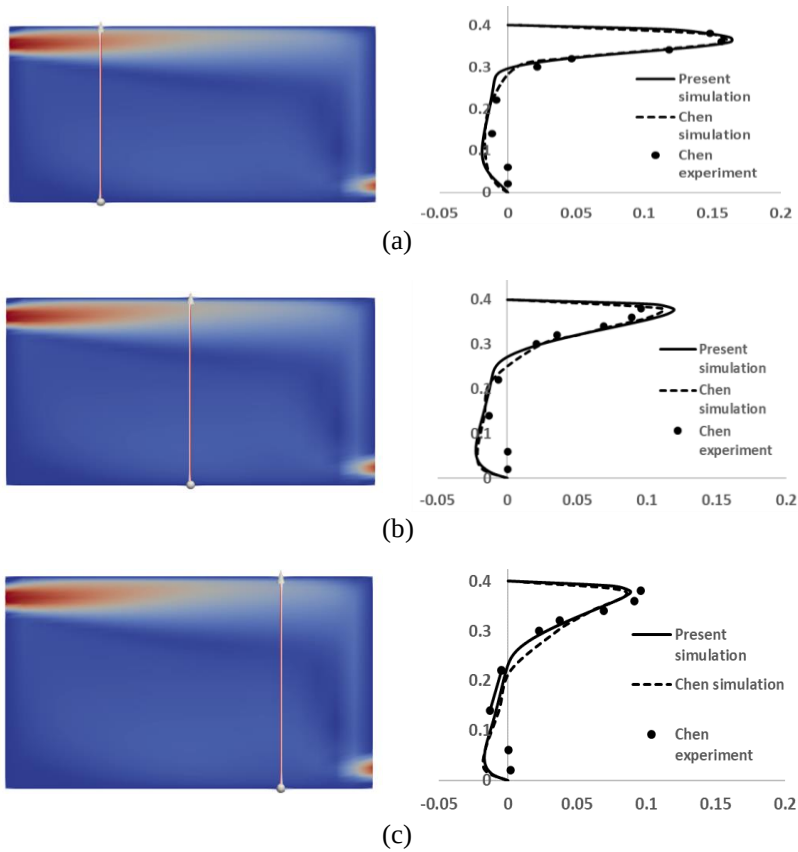

Figure 4: The contour of velocity (inlet velocity 0.225 ms^{-1}) and the comparison of measured and predicted x direction velocities at three different locations [10]; (a) x=0:2 m, (b) 0.4 m, and (c) 0.6 m

Validation metrics

The factor of two observations (FAC2), the factor of 1.3 observations (FAC1.3), the normalised mean square error (NMSE), and the fractional bias (FB) are four validation metrics used in this study to acquire a quantitative assessment of the performance of the chosen RANS turbulence models [12], [40]. In addition, every turbulence model's statistical performance is assessed in terms of streamwise velocity [21], [41]. These models include STD k

epsilon, RNG k epsilon, RLZ k epsilon, and SST k omega. Metrics are computed via Equations (11), (12), (13), and (14).

$$FAC2 = \frac{1}{N}\sum_{i=1}^{N} n_i \ \ with\, n_i = \begin{cases} 1, for\ \ 0.5 \le \dfrac{P_i}{O_i} \le 2 \\ 0, else \end{cases} \tag{11}$$

$$FAC1.3 = \frac{1}{N}\sum_{i=1}^{N} n_i \ \ with\, n_i = \begin{cases} 1, for\ \ 0.77 \le \dfrac{P_i}{O_i} \le 1.3 \\ 0, else \end{cases} \tag{12}$$

$$FB = \frac{[O] - [P]}{0.5\,([O] + [P])} \tag{13}$$

$$NMSE = \frac{(\overline{O_i - P_i}).^2}{\overline{O_i}\,\overline{P_i}} \tag{14}$$

with P_i as the predicted value (Chen's simulation [10]), O_i as the observed (present simulation/measured) value, and n as the number of measurement locations, equal to 32 for three different locations. The overbar denotes averaging over the whole dataset. Table 3 depicts the results for velocities along three vertical lines (x=0.2, 0.4, and 0.6). The ideal values correspond to a perfect agreement between Chen's simulation and the present simulation result in which FAC2=1, FAC1.3=1, FB=0, and NMSE=0. FAC counts the fraction of data points where the predictions are within 2 or 1.3 of the observations based on the predicted and observed value ratio. FB is a linear measure of the mean bias and reveals systematic errors.

Table 3: Validation metrics for x-velocity for present simulation with Chen's simulation

Present simulation vs.	FAC2	FAC1.3	FB	NMSE
Chen's simulation [10]	0.7813	0.6875	-0.446	0.00358
Ideal values	1	1	0	0

FAC2 for all lines was 0.7813, and FAC1.3 was 0.6875, near the ideal value of 1. FB value showed an underestimate of the present simulation than the predicted value, which was -0.446 and near the ideal value of 0. Meanwhile, NMSE showed a value of 0.00358 which was slightly near the ideal value of 0. This indicates that the observed data agrees well with Chen's simulation data. Figure 5 shows a scatter plot of measured versus modelled values for horizontal, along with three velocity components, *Ux*. Again, all data points (32) in the vertical profiles are included.

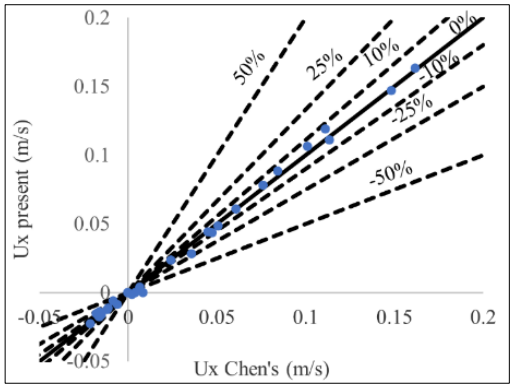

Figure 5: Compares the present and Chen's [10] simulation results in three locations. As indicated, black dotted lines correspond to 10%, 25%, and 50% errors

Turbulence model verification

Four RANS models are used to simplify the calculations in this paper for the validation simulation. The 3D steady RANS (Reynolds-Average Navier Stokes) equation is solved using the combination of four turbulence models: two-equation eddy viscosity models such as renormalization group *k* epsilon model (RNG *k*-ε), standard *k* epsilon model (STD *k*-ε), realizable *k* epsilon model (RLZ *k*-ε), and shear stress transport k omega (SST *k*-ω). The statistical performance of every turbulence model is evaluated. However, RLZ *k*-ε and SST *k*-ω are not converged.

Figure 6 compares the graph of Chen's [10] simulation and the present simulation of RNG *k*-ε and STD *k*-ε model. Table 4 shows the validation metrics for *x*-velocity for both turbulence models RNG and STD *k*-ε model. FAC2 for RNG *k*-ε and STD *k*-ε were 0.47 and 0.53, while the ideal value for FAC2 was 1.

Table 4: Validation metrics of x-velocity for RNG and STD *k* epsilon model simulation with Chen's simulation

	FAC2	FAC1.3	NMSE
RNG *k* epsilon	0.47	0.4	0.00025
STD *k* epsilon	0.53	0.4	0.00017
Ideal values	1	1	0

Both turbulence model values for FAC1.3 were 0.4, where the ideal value is 1. NMSE values were 0.00025 and 0.00017 for RNG *k*-ε and STD *k*-ε, which is slightly near to the ideal value of 0. This indicates that the observed

data agrees better with STD *k-ε* simulation data. Figures 7 and 8 show the scatter plot of measured versus modelled values for horizontal, along with three velocity components, *Ux* for RNG *k-ε* and STD *k-ε* model, as compared with Chen's simulation [10].

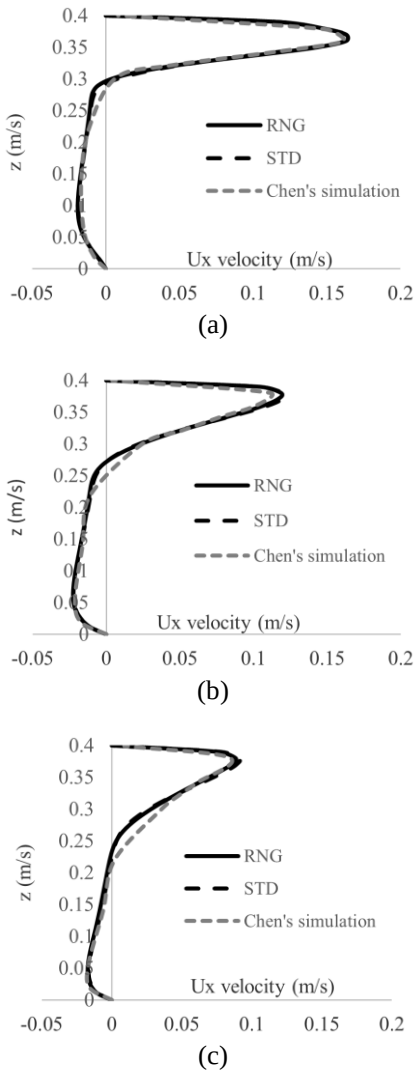

Figure 6: Compares the present and Chen's simulation [10] results in STD *k* epsilon turbulence model. As indicated, black dotted lines correspond to 10%, 25%, and 50% errors

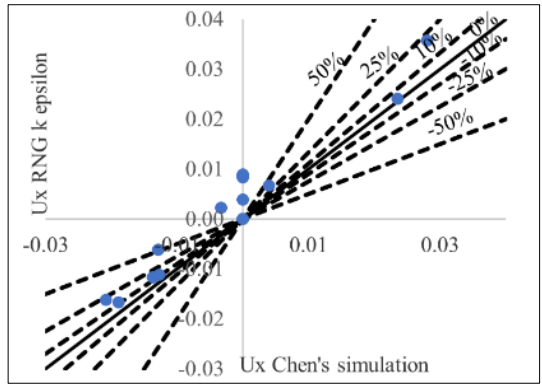

Figure 7: Compares the present and Chen's simulation [10] results in RNG *k* epsilon turbulence model. As indicated, black dotted lines correspond to 10%, 25%, and 50% errors

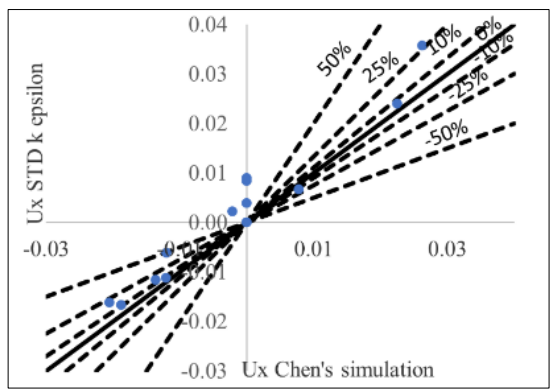

Figure 8: Compares the present and Chen's simulation [10] results in STD *k* epsilon turbulence model. As indicated, black dotted lines correspond to 10%, 25%, and 50% errors

Grid refinement

The research on grid refinement was performed on each of the three grid resolutions. The grid size in Example A is the largest, the resolution in Case B is medium, and the resolution in Case C is the finest [21]. Case A has the coarsest grid, Case B has the medium resolution, and Case C has the finest resolution. These cases are shown in Table 5 for their specification while Figure 10 depicts their visualization. By increasing the grid size the domain is discretized into coarse, medium, and fine grids. This results in a total grid

number of 1,414,933, 3,981,287, and 5,668,675, along with their respective computing times.

Table 5: Specification case for coarse, medium, and fine grid

Case	A (Coarse)	B (Medium)	C (Fine)
Number of cells	1 414 933	3 981 287	5 668 675
Computation time	03 h 36 m 06	24 h 50 m 21	48 h 18 m 02

Truncation error decreased with grid number. Mesh type had little effect on simulation outcomes at large grid numbers [14]. Figure 13 compares simulated and measured airflow distributions with coarse (1 million cells), medium (3 million cells), and fine (5 million cells) meshes at a room cross-section. Figure 11(a) shows the cross-section location.

Velocity contour and streamlines

Figure 9 shows the schematic of the room geometry for the *xy*-plane. Figure 10 shows the velocity contour for three different grid sizes measured at the *xy*-plane, where room height, z=1, and room width, x=2, are at the central location of the domain. It shows that the coarse grid is different from the medium and fine grids. It shows the medium and fine grids are slightly the same.

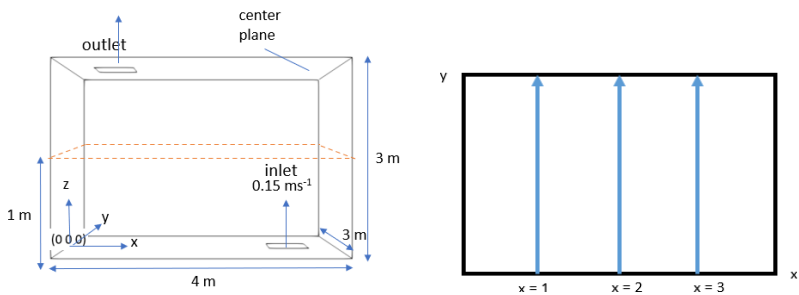

Figure 9: a) Schematic of the room geometry at xy-plane, and b) line at *xy*-plane

Figure 11 shows the velocity profile for the three cases. The horizontal axis represents the x velocity, Ux, while the vertical axis indicates the room length, y. It shows the symmetrical flow velocity for both sides of the room length at three-line positions x=2, x=6, and x=8. This result was taken at the room's height of z=1 m. It was considered for the sitting position. At lines x=2 and x=4, in the middle of the room, the flow velocity is the highest compared to both sides of the room. When x=6, the velocity profile shape is different and near zero velocity.

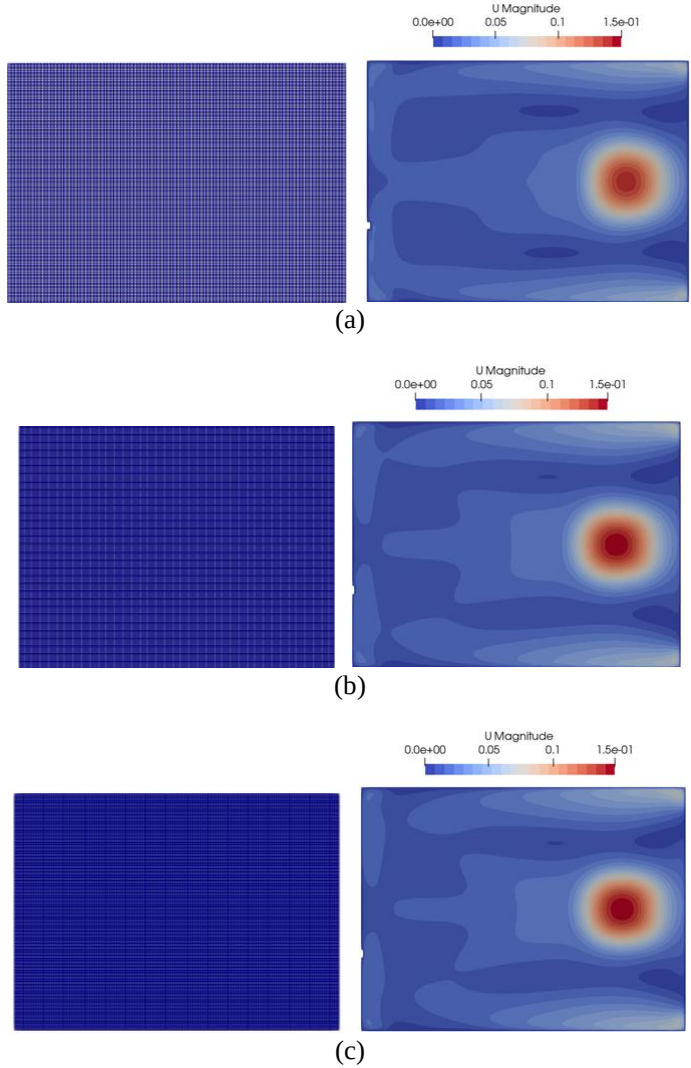

Figure 10: Block mesh and geometry structure with velocity contour for different cases: at the *x-y* plane, *z*=1, at the middle domain; (a) coarse, (b) medium, and (c) fine

The profile also shows that a significant difference can be observed for the coarse mesh (dashed line) compared to medium (solid line), while less significant for medium (solid line) and fine (dotted line) grids. Similar velocity profiles can be found using either a medium or fine grid. Due to the nearly

grid-independent nature of the medium grid's output, it is selected for further simulations [10], [42]-[43]. The GCI is a metric for determining the degree of grid convergence. Figure 11 also shows the mean error for medium and fine mesh, where line x=2 is 0.14% error, x=4 is 0.08% error, and x=8 is 0.09% error. The difference between medium mesh and fine, as shown, is accepted. Therefore, the computational time for medium mesh is acceptable for simulation. Overlooked will add a level of complexity, which makes the whole process of prototype or numerical modelling almost unsolvable.

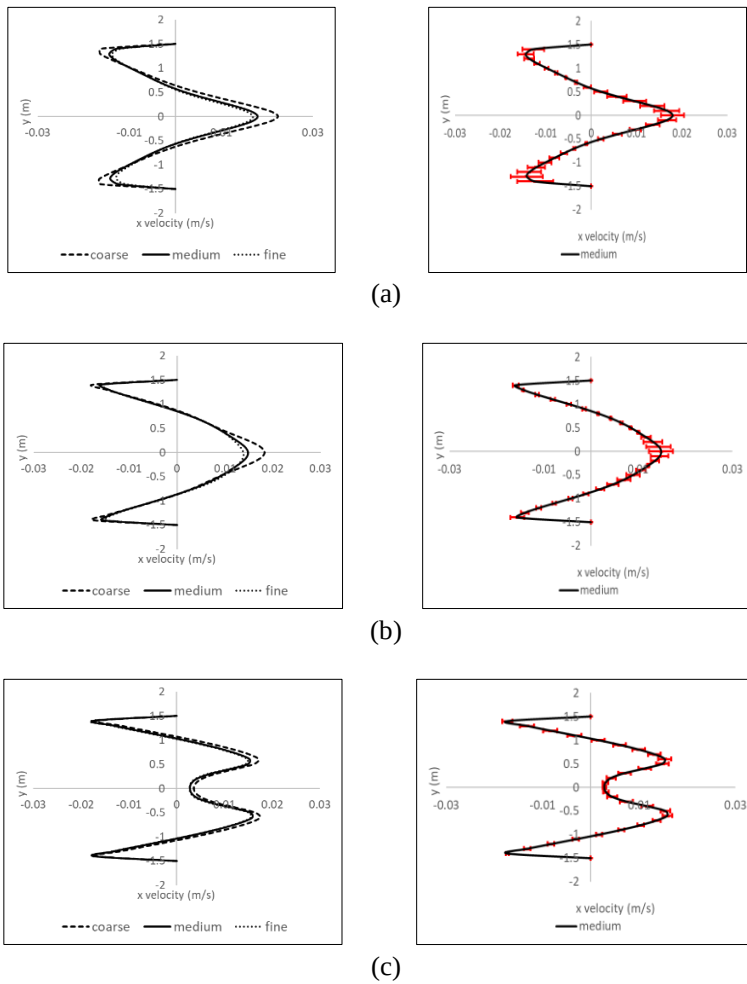

Figure 11: Velocity profile and graph with error bar to compare the medium and fine mesh at the x-y plane, (a) x=2, (b) x=4, and (c) x=6

Conclusion

Computational fluid dynamics (CFD) is an efficient tool for analysing airflow in a built-in environment. To sustain the quality of CFD simulations, the process of numerical modelling must be appropriately governed; this is becoming an essential supplementary to experimental and theoretical methods. CFD numerical data can explain airflow performance in terms of air quality, occupants' thermal comfort, and building energy savings. Consequently, this work presents turning CFD analyses of indoor airflow in the building environment. The performance of CFD modelling is investigated in terms of the efficiency of computational grids, convergence criteria, and validation techniques. More often, numerical models are used to show how natural processes work. Since we have improved numerical tools, it is possible to describe the behaviour of complex flow phenomena more precisely. Even though more complicated systems can be solved, there is still some assumption about how accurate the solutions are. Putting the results of experiments and simulations next to each other is not enough to prove how good the outcome is. CFD problems can be solved via a variety of mesh-independent solution approaches. The most well-known methods are Grid Resolution, General Richardson Extrapolation, and Grid Convergence Index techniques. The Grid Convergence Index (GCI) methodology provides a way to calculate and report discretization error estimates in CFD simulations. It lets us measure how much uncertainty there is in grid convergence. Solutions on three distinct grids are provided to study the effect of the numerical scheme, boundary conditions, and grid independence. Using a kind of Richardson extrapolation, the level of grid independence is determined, and the analysis reveals that the optimal grid solution has a Grid Convergence Index (GCI) of less than 5%. Due to a satisfactory correlation, the suggested method is successfully validated compared to experimental results in the scientific literature [10]. These results are verified with four validation metrics to gain a quantitative assessment of the performance of the chosen RANS turbulence models: FAC2, FAC1.3, NMSE, and FB. The result of FAC2, FAC1.3, FB, and NMSE is accepted. With an increasing number of mesh revisions, this method's implementation will yield better results. In addition, to successfully deliver a mesh-independent solution, the method avoids the difficulties and expenses associated with conducting experiments for extremely small meshes. The main goal of grid convergence studies is to find the best grid size so that the accuracy of the answer is not affected by the size of the computational grid. The number of cells and the amount of time it takes to do the calculations are both related. Increasing the grid density to get better results will increase the amount of time it takes to do the calculations. So, a grid convergence study is a test that needs to be done to reduce the amount of time it takes to solve a problem without sacrificing the accuracy of the answer. The results here let us choose the right

mesh for future or more complicated simulations involving airflow in buildings.

Contributions of Authors

The authors confirm the equal contribution in each part of this work. All authors reviewed and approved the final version of this work.

Funding

This research was financially supported by UiTM Lestari COVID Research Grant (600-RMC/LESTARI COVID/5/3 (010/2020)).

Conflict of Interests

All authors declare that they have no conflicts of interest

Acknowledgement

First and foremost, I would like to sincerely thank my main supervisor, Assoc. Prof. Ir. Ts. Dr. Azli Abd Razak, my co-supervisors, Dr. Fauziah Jerai, Ir. Dr. Mohamed Azly Abdul Aziz, and my lecturer Dr. Mohd Faizal Mohamad for their guidance and understanding. Most importantly, they provided positive encouragement and a warm spirit to do the study. This paper publication fee is supported by College of Engineering Universiti Teknologi MARA.

References

[1] J. Gao, H. Wang, X. Wu, F. Wang, and Z. Tian, "Indoor air distribution in a room with underfloor air distribution and chilled ceiling: Effect of ceiling surface temperature and supply air velocity", *Indoor and Built Environment*, vol. 29, no. 2, pp. 151–162, 2020. doi: 10.1177/1420326X19853605.

[2] M. P. Wan and C. Y. Chao, "Numerical and experimental study of velocity and temperature characteristics in a ventilated enclosure with underfloor ventilation systems", *Indoor Air*, vol. 15, no. 5, pp. 342–355, 2005. doi: 10.1111/j.1600-0668.2005.00378.x.

[3] S. J. Cao and C. Ren, "Ventilation control strategy using low-dimensional

linear ventilation models and artificial neural network", *Building and Environment*, vol. 144, pp. 316–333, 2018. doi: 10.1016/j.buildenv.2018.08.032.

[4] S. Schiavon, D. Rim, W. Pasut, and W. W. Nazaroff, "Sensation of draft at uncovered ankles for women exposed to displacement ventilation and underfloor air distribution systems", *Building and Environment*, vol. 96, pp. 228–236, 2016. doi: 10.1016/j.buildenv.2015.11.009.

[5] N. P. Gao and J. L. Niu, "Modeling particle dispersion and deposition in indoor environments", *Atmospheric Environment*, vol. 41, no. 18, pp. 3862–3876, 2007. doi: 10.1016/j.atmosenv.2007.01.016.

[6] A. C. K. Lai and F. Chen, "Modeling particle deposition and distribution in a chamber with a two-equation Reynolds-averaged Navier-Stokes model", *Journal of Aerosol Science*, vol. 37, no. 12, pp. 1770–1780, 2006. doi: 10.1016/j.jaerosci.2006.06.008.

[7] L. K. Moey, N. M. Adam, and K. A. Ahmad, "Effect of venturi-shaped roof angle on air change rate of a stairwell in tropical climate", *Journal of Mechanical Engineering.*, vol. SI 4, no. 4, pp. 135–150, 2017.

[8] A. Murga, S. J. Yoo, and K. Ito, "Multi-stage downscaling procedure to analyse the impact of exposure concentration in a factory on a specific worker through computational fluid dynamics modelling", *Indoor and Built Environment*, vol. 27, no. 4, pp. 486–498, 2018. doi: 10.1177/1420326X16677331.

[9] S. J. Cao, "Challenges of using CFD simulation for the design and online control of ventilation systems," *Indoor and Built Environment*, vol. 28, no. 1, pp. 3–6, 2019. doi: 10.1177/1420326X18810568.

[10] F. Chen, S. C. M. Yu, and A. C. K. Lai, "Modeling particle distribution and deposition in indoor environments with a new drift-flux model", *Atmospheric Environment*, vol. 40, no. 2, pp. 357–367, 2006. doi: 10.1016/j.atmosenv.2005.09.044.

[11] H. lin Liu, M. ming Liu, Y. Bai, and L. Dong, "Effects of mesh style and grid convergence on numerical simulation accuracy of centrifugal pump", *Journal of Central South University*, vol. 22, no. 1, pp. 368–376, 2015. doi: 10.1007/s11771-015-2531-9.

[12] P. Cardiff, "Introduction to Meshing in OpenFOAM," *University College Dublin*, p. 70, 2017.

[13] G. Park, C. Kim, M. Lee, and C. Choi, "Building geometry simplification for improving mesh quality of numerical analysis model", *Applied Sciences*, vol. 10, no. 16, pp. 1-18, 2020. doi: 10.3390/APP10165425.

[14] N. Baker, G. Kelly, and P. D. O'Sullivan, "A grid convergence index study of mesh style effect on the accuracy of the numerical results for an indoor airflow profile", *International Journal of Ventilation*, vol. 19, no. 4, pp. 300–314, 2020. doi: 10.1080/14733315.2019.1667558.

[15] J. Franke, A. Hellsten, H. Schlünzen, and B. Carissimo, "Best Practice Guideline for the Cfd Simulation of Flows in the Urban Environment.

Cost 732: Quality Assurance and Improvement of Microscale Meteorological Models", in *COST Action C14: Impact of Wind and Storm on City Life and Urban Environment*, 2007.

[16] R. Duan *et al*., "Mesh type and number for the CFD simulations of air distribution in an aircraft cabin", *Numerical Heat Transfer, Part B: Fundamentals,*, vol. 67, no. 6, pp. 489–506, 2015. doi: 10.1080/10407790.2014.985991.

[17] F. M. Sakri, M. S. M. Ali, and S. A. Z. S. Salim, "Computational investigations and grid refinement study of 3D transient flow in a cylindrical tank using OpenFOAM", *IOP Conference Series: Materials Science and Engineering*, vol. 152, no. 1, pp. 1-13, 2016. doi: 10.1088/1757-899X/152/1/012058.

[18] M. M. Hefny and R. Ooka, "CFD analysis of pollutant dispersion around buildings: Effect of cell geometry", *Building and Environment*, vol. 44, no. 8, pp. 1699–1706, 2009. doi: 10.1016/j.buildenv.2008.11.010.

[19] L. Kang and T. van Hooff, "Influence of inlet boundary conditions on 3D steady RANS simulations of non-isothermal mechanical ventilation in a generic closure", *International Journal of Thermal Sciences*, vol. 182, p. 107792, 2022. doi: 10.1016/j.ijthermalsci.2022.107792.

[20] H. Mohammed and A. Belkacem, "Convergence order prediction of CVFEM solutions using the richardson extrapolation method on unstructured grids", *Journal of Advanced Research in Fluid Mechanics and Thermal Sciences*, vol. 67, no. 2, pp. 27–39, 2020.

[21] S. Gilani, H. Montazeri, and B. Blocken, "CFD simulation of stratified indoor environment in displacement ventilation: Validation and sensitivity analysis", *Building and Environment*, vol. 95, pp. 299–313, 2016. doi: 10.1016/j.buildenv.2015.09.010.

[22] Y. Wu, L. Feng, M. Liu, Z. Wu, and N. Gao, "Numerical study on transient airflows and air exchange induced by door motion in thermally stratified environment", *Building and Environment*, vol. 223, p. 109498, 2022. doi: 10.1016/j.buildenv.2022.109498.

[23] D. Prakash and P. Ravikumar, "Analysis of thermal comfort and indoor air flow characteristics for a residential building room under generalized window opening position at the adjacent walls", *International Journal of Sustainable Built Environment*, vol. 4, no. 1, pp. 42–57, 2015. doi: 10.1016/j.ijsbe.2015.02.003.

[24] H. Motamedi, M. Shirzadi, Y. Tominaga, and P. A. Mirzaei, "CFD modeling of airborne pathogen transmission of COVID-19 in confined spaces under different ventilation strategies", *Sustainable Cities and Society*, vol. 76, p. 103397, 2022. doi: 10.1016/j.scs.2021.103397.

[25] Á. L. De Bortoli, G. S. L. Andreis, and F. N. Pereira, "Numerical Methods for Reactive Flows", in Modeling and Simulation of Reactive Flows, Elsevier, 2015.

[26] R. Viswanath, and Y. Jaluria "A Comparison of Different Solution

Methodologies For Melting and Solidification Problems in Enclosures", *Numerical Heat Transfer , Part B : Fundamentals*, vol. 24, no. 1, pp. 77-105, 2007.

[27] S. Kato, "Review of airflow and transport analysis in building using CFD and network model", *Japan Architectural Review*, vol. 1, no. 3, pp. 299–309, 2018. doi: 10.1002/2475-8876.12051.

[28] H. Jasak, "Error analysis and estimation for finite volume method with applications to fluid flow", PhD Thesis, 1996.

[29] ICOP-IAQ, "Industry Code of Practice on Indoor Air Quality", Ministry Human Resource Department Occupational Safety Health, 2010.

[30] P. J. Roache, "Perspective: A Method for Uniform Reporting of Grid Refinement Studies", *Journal of Fluid Engineering*, vol. 116. pp. 405–413, 1994.

[31] T. S. Phillips, "Extrapolation-based Discretization Error and Uncertainty Estimation in Computational Fluid Dynamics Extrapolation-based Discretization Error and Uncertainty Estimation in Computational Fluid Dynamics", M.S. thesis, Aero. Eng., Virginia Polytech. and State Univ., Virginia, Feb. 2012, [Online]. Available: https://vtechworks.lib.vt.edu/handle/10919/31504.

[32] R. Castedo et al., "Application of grid convergence index to shock wave validated with LS-DYNA and ProsAir", *Ingenieria e Investigacion*, vol. 39, no. 3, pp. 20–26, 2019. doi: 10.15446/ing.investig.v39n3.81380.

[33] A. Alañón, E. Cerro-Prada, M. J. Vázquez-Gallo, and A. P. Santos, "Mesh size effect on finite-element modeling of blast-loaded reinforced concrete slab", *Engineering with Computers*, vol. 34, no. 4, pp. 649–658, 2018. doi: 10.1007/s00366-017-0564-4.

[34] S. R. Lizarose Samion, N. H. Shaharuddin, and M. S. Mat Ali, "Grid Convergence Study for Detached-Eddy Simulation of Flow over Rod-Airfoil Configuration Using OpenFOAM", *IOP Conference Series: Materials Science and Engineering*, vol. 491, no. 1, pp. 1-7, 2019. doi: 10.1088/1757-899X/491/1/012023.

[35] P. J. Roache, "Quantification of uncertainty in computational fluid dynamics", *Annual Review of Fluid Mechanics*, vol. 29, pp. 123–160, 1997. doi: 10.1146/annurev.fluid.29.1.123.

[36] V. Carrillo, J. Petrie, and E. Pacheco, "Application of the grid convergence index to a laminar axisymmetric sudden expansion flow", *Universidad de Cuenca*, pp. 115–123, 2015.

[37] L. E. Schwer, "Is your mesh refined enough? Estimating Discretization Error using GCI", *7th LS-DYNA Anwenderforum*, vol. 1, no. 1, pp. 45–54, 2008.

[38] L. Kwasniewski, "Application of grid convergence index in FE computation", *Bulletin of the Polish Academy of Sciences: Technical Sciences*, vol. 61, no. 1, pp. 123–128, 2013. doi: 10.2478/bpasts-2013-0010.

[39] M. Sukri and M. Ali, "Validation study on external wind noise prediction using OpenFOAM", *Journal of Mechanical Engineering*, vol. 15, no. 1, pp. 111–126, 2018.

[40] M. . Ibrahim, M. . Mohamad, N. Ikegaya, and A. A. Razak, "Numerical Investigation on the Effect of Building Overhang on the Flow within Idealised Two-dimensional Street Canyon", *ESTEEM Academic Journal*, vol. 17, no. 11, pp. 67–77, 2021.

[41] M. A. Zainol *et al*., "The effect of urban obstacles on the flow distribution at pedestrian area", *IOP Conference Series: Materials Science and Engineering*, vol. 834, no. 1, pp. 1-7, 2020. doi: 10.1088/1757-899X/834/1/012023.

[42] S. Giersch and S. Raasch, "How Do Dust Devil-Like Vortices Depend on Model Resolution? A Grid Convergence Study Using Large-Eddy Simulation", *Boundary-Layer Meteorology*, vol. 187, no. 3, pp. 703–742, 2023. doi: 10.1007/s10546-023-00792-3.

[43] Y. Zhao and X. Su, "IMM FSI Model Validations and Applications for Compressible Flows", in *Computational Fluid-Structure Interaction*, Academic Press, Elsevier, pp. 355-408, 2019.